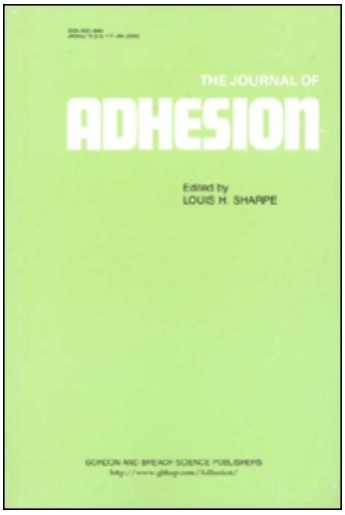

The Journal of Adhesion
Publication details, including instructions for authors and subscription information:
http://www.informaworld.com/smpp/title~content=t713453635

Nanoscale Mechanical Characterization of the Effect of Thermal Aging on Titanium/PETI-5 Adhesive Interface Properties

James D. Holbery[ab]; Robert M. Fisher[a]
[a] Department of Materials Science and Engineering, University of Washington, Seattle, WA, USA [b] CSEM Instruments SA, neuch, Switzerland

To cite this Article Holbery, James D. and Fisher, Robert M.(2001) 'Nanoscale Mechanical Characterization of the Effect of Thermal Aging on Titanium/PETI-5 Adhesive Interface Properties', The Journal of Adhesion, 76: 2, 93 — 121
To link to this Article: DOI: 10.1080/00218460108029620
URL: http://dx.doi.org/10.1080/00218460108029620

J. Adhesion, 2001, Vol. 76, pp. 93–121
Reprints available directly from the publisher
Photocopying permitted by license only

Nanoscale Mechanical Characterization of the Effect of Thermal Aging on Titanium/PETI-5 Adhesive Interface Properties

JAMES D. HOLBERY* and ROBERT M. FISHER

Department of Materials Science and Engineering, University of Washington, Seattle, WA 98195, USA

(Received 1 August 2000; In final form 22 December 2000)

Titanium substrates coated with silicate/zirconate sol-gel and plasma sputtered chromium have been adhered using a combined PETI-5 polyimide psuedo-thermoplastic primer/adhesive system. Composite laminates were exposed to thermal aging up to 2000 hours at 194°C and subsequently nanoindentation testing was performed across each interface to determine material modulus degradation and plastic deformation changes. The procedure to analyze complex interfaces using nanoindentation are explained in detail including experimental set-up, analysis, and imaging; for example, inhomogeneities at the interface mandated that both low loads (as low as 25 μN) and a 90° cube-corner diamond tip be utilized to obtain sub-micron resolution. Thermal aging resulted in an increase in PETI-5 primer and adhesive modulus by 15% and upwards of 30%, respectively, and the sol-gel modulus increased by approximately 10%. An exposure level at 1000 hours showed a 20% increase in the chromium modulus. Large increases in plastic deformation were observed in the polymeric materials likely due to chain embrittlement.

Keywords: Adhesion; Composite; Interface; Nanoindentation; Thermal aging; Thermoplastic; Titanium

*Present address: CSEM Instruments SA, Jaquet-Droz 1, CH-2007, Neuchâtel, Switzerland. Tel.: 41 32 720 5847, Fax: 41 32 720 5730, e-mail: james.holbery@csem.ch

1. INTRODUCTION

1.1. General

Structural adhesives have shown an increase in usage in many industries due in part to advantages offered over conventional fasteners such as rivets and bolts. The High Speed Civil Transport (HSCT), currently researched by NASA, proposes an air speed capability of Mach 2.4 combined with an operating temperature of 177°C. The operating environment is more severe than conventional subsonic air transport vehicles due to high temperatures associated with the aerodynamic friction heating caused by supersonic cruise speeds. If supersonic transport is to be economically feasible under stringent operating conditions, such as a service life of 60,000 hours combined with a 30% weight reduction relative so the Concorde, new alloys and bonded composite structures must maintain strength and durability while minimizing the weight and the cost impact of manufacturing processes.

The fraction of the operating empty weights for a supersonic airframe structure is significantly less as compared with conventional subsonic commercial vehicles requiring the use of innovative structural concepts and advanced materials to satisfy stringent weight requirements. Conventional aerospace materials such as aluminum and bismaleimide thermoset composites do not possess the temperature capability necessary for this aircraft and titanium alloys are too heavy for the entire airframe. Thus, bonded titanium structures are a design consideration for the HCST due to the ability to achieve high structural efficiency resulting from large load introduction areas achievable with structural bonding.

A patented series of phenylethynyl-terminated imide oligomers have been developed by NASA Langley to offer high toughness and thermo-oxidative stability for long-term structural applications at elevated temperatures and has been the basis for composite resins and adhesives considered for bonding applications on the HSCT [1–5]. FM-5, a modified adhesive based on the PETI-5 version of molecular weight of 2500 g/mol, has been formulated by Cytec Industries Inc. (Havre de Grace, MD, USA). It is composed of a proprietary polyimide with a small amount of fused silica (Cytec Fiberite FR x5

based on NASA PETI-5, Tg$\sim$250°C) and applied to a woven glass scrim pretreated with aminopropylsilane. The adhesive is applied in conjunction with PETI-5 primer (Cytec Fiberite BR x5), a dilute solution of the NASA LaRC PETI-5 polyimide with additives for handling purposes applied in thicknesses ranging from 100–200 nm [6].

The two crystallographic forms of titanium, hexagonal close-packed alpha phase and body-centered cubic beta phase, may be manipulated through alloying additions and thermo-mechanical processing to produce a wide range of properties. Titanium alloys considered in this study are Ti-6Al-4V (Ti-6-4) and Ti-15V-3Cr-3Al-3Sn (Ti-15-3-3-3). While Ti-6-4 is widely used in the annealed form with an ultimate tensile strength (UTS) of 895 MPa, Ti-15-3-3-3 is a beta alloy developed to be cold-formable yet heat treatable to achieve a UTS above 1 GPa. Two groups of elements stabilize the beta crystal structure by lowering the transformation temperature [7]. The beta isomorphous group consists of elements miscible in the beta phase including molybdenum, vanadium, tantalum, and niobium while the other forms eutectoid systems with titanium resulting in eutectoid temperatures as much as 333°C below the transformation temperature of unalloyed titanium. The high-temperature and high-strength eutectoid additives in Ti-15-3-3-3 include manganese, iron, chromium, cobalt, nickel, copper, and silicon and enable a reduction of wall thickness and weight savings in high temperature applications [8].

Two coatings selected as potential gradient materials between the metallic substrate and organic resin are a combination silicate/zirconate sol-gel and a plasma-sputtered chromium. Substrates prepared prior to sol-gel application are grit blasted followed by a nitric/HF acid etch.

Aliphatic sol-gel coating is formed by creating a low-concentration solution of aminopropyltrimethoxysilane (APS) and zirconium n-propoxide in water. The pH conditions are manipulated enabling the APS and zirconate to hydrolyze and partially polymerize. The solution is applied to the titanium substrate, allowed to air dry, then baked at 125°C to initiate the hydrolyzed silane and zirconate to undergo a condensation reaction and form a mixed organic/inorganic matrix with covalent bonds to the titanium oxide substrate. The goal of this process is to remove the hydroxide groups completely, leaving only the

amine organic functionality to react the amine with polyamic acid primer to form a direct chain of covalent bonds between the adhesive and titanium substrate.

Chromium is applied to a previously chemically etched titanium substrate in a high-vacuum atmosphere at a thickness of 1000 Å. Prior to sputtering, the titanium substrate is plasma sputtered to remove native titanium oxide rendering a clean metallic titanium surface. This process takes advantage of a unique affinity for chromium oxide that polyimides exhibit.

Several factors affect long-term adhesive stability, although the interfacial region between a polymer and substrate is commonly thought to be critical in predicting system performance [9–11]. Physical aging as a result of interface environmental exposure accelerates time-dependent changes in volume, enthalpy and entropy, as well as decrease in mechanical properties [12, 13]. This physical phenomenon is increased drastically when a large coefficient of thermal expansion at the interface material exists. The combined effects of physical and chemical aging of the systems described herein have been examined and it was found that physical aging begins at the outset of exposure and continues to progress, while the effects of chemical aging began with increased exposure time [14]. The present work aims to measure the nano-mechanical properties of bonded titanium-PETI-5 adhesive laminates currently under consideration for structural applications on the HSCT and quantify the nano-mechanical degradation due to thermal aging at the interface.

1.2. Nano-mechanical Testing

Nanomechanical analysis has proven an effective means to determine the properties of thin surface layers on devices such as magnetic disk recording media and other media [15, 16]. The mechanical properties of materials in nanoscale dimensions can be different from bulk material of the same composition due to localized microstructure anomalies, grain size, dislocation spacing, or the effect of dimensional constraints. Nanoindentation is useful for studying the adhesion of thin films by determining properties such as film hardness, modulus, residual stress, and time-dependent characteristics. Localized properties are obtained as an indenter is forced into a material while the

displacement from both elastic and plastic deformation is recorded. When the indenter is removed, a residual indentation may remain.

In these experiments, a scanning probe microscope (Model CP, ThermoMicroscopes, Palo Alto, CA, USA) combined with a Hysitron® Nanoindentation transducer and associated software (Hysitron Inc., Minneapolis, MN, USA) has been utilized. Instruments mounted on a multi-layer vibration pad were situated in a room maintained at 20°C ± 2°C. Contact Scanning Probe Microscopy (SPM) images were acquired using a diamond indentation tip in constant-force mode. Additional SPM images were acquired using a Digital Instruments Nanoscope III (Digital Instruments, Santa Barbara, CA, USA) in both contact and tapping modes.

The Hysitron® Nanoindentation transducer consists of three parallel plates forming two capacitors with the middle plate suspended by springs between the rigidly fixed outer two. The indenter tip is attached to the middle of the center plate and passes through the lower plate *via* a small hole. A force is applied to the center plate by applying a voltage, V_f, between the center and lower plates with the displacement measured at the same time by monitoring the capacitance between the center and upper plates [17]. This simultaneous measurement of force and displacement provides the ability to produce quantitative force-displacement curves [18].

Nanoindentation analysis based on the elastic contact model was addressed initially by workers at the Baikov Institute of Metallurgy in Moscow during the 1970's [19], though the first practical method was presented by Doerner and Nix [20] and subsequently refined by Oliver and Pharr [21]. The method is based on the assumptions that Young's modulus of elasticity is independent of indentation depth, deformation upon unloading is purely elastic, and sample compliance and the indenter tip may be combined as springs in series as follows:

$$\frac{1}{E_r} = \left(\frac{1 - \nu_i^2}{E_i}\right) + \left(\frac{1 - \nu_m^2}{E_m}\right) \tag{1}$$

where E_r is the "reduced modulus", E is Young's modulus, ν is Poisson's ratio and i and m refer to the indenter and tested material, respectively. In an effort to solve for the material modulus, the initial

slope of the unloading curve is measured by:

$$S = \frac{dP}{dh} = \frac{2}{\sqrt{\pi}} E_r \sqrt{A} \tag{2}$$

where S is the measured stiffness and A the contact area [22]. This equation relates the reduced modulus, E_r, to both the contact area and measured stiffness.

1.3. Indenter Tip Geometry

Several different indenter geometries exist, including conical, spherical, and blunt tips that generally eliminate cutting material due to sliding along the tip-sample interface. Sharp tips such as Berkovich, Vickers, and the cube-corner insure localized deformation. The most common tip shape used is the Berkovich indenter, a 3-sided pyramid with a very similar projected area/face area ratio to the Vickers 4-sided pyramid (0.927 *versus* 0.908, respectively) [23].

Measurements initially obtained in this study used a Berkovich diamond tip. Imaged indentations indicate that a sharp Berkovich tip radius does not produce sufficiently small material impressions to obtain the resolution required to analyze very thin interfaces. The actual curvature of this Berkovich tip has been determined using a Field Emission Scanning Electron Microscope (FESEM, Joel Model JSM 630F) and is approximately 150 nm, although it is difficult to determine exact dimensions from the view in Figure 1a. Recently, one group has reported Berkovich tips with a radius of 23 nm [24].

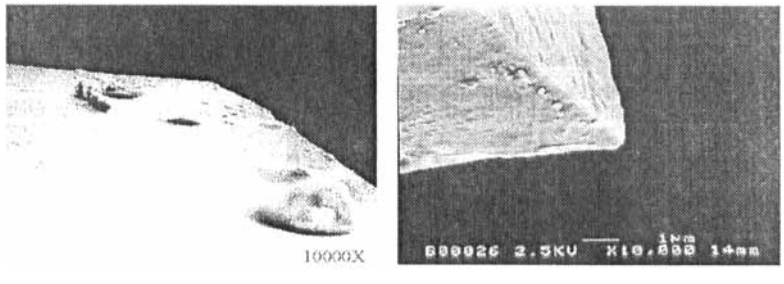

FIGURE 1 (a) Three-sided Berkovich with tip radius estimated at 150 nm. (b) 90° cube corner tip with radius estimated at 120 nm.

The radius of the 90° cube-corner tip used in this study was reported to be between 30–50 nm by the manufacturer, though the actual curvature of the tip as determined by FESEM is approximately 100 nm (Fig. 1b). One is able to view a slight imperfection at the tip end corresponding with reports in the literature claiming typical "sharp" cube-corner tip radii are on the order of 100 nm [25].

Depending on the material tested, diamond tips may become contaminated upon repeated use. When this occurs, results and indentation images will be dramatically altered. In our experimental procedure, after the completion of every fifth series of measurements a fused silica standard was indented and subsequently imaged, with the resulting modulus value and the image being compared with a known standard for clarification. Additionally, the tip was re-examined with the FESEM after approximately 200 indents to evaluate its quality. Figure 2 depicts a used 90° cube-corner tip with material deposits clearly evident.

Tip shape is critical to achieve maximum image clarity. Generally, a blunt tip eliminates cutting of material due to sliding along the tip/sample interface. Sharp tips ensure localized deformation and are applicable to the contact model for small indentation depths. This is a trade off, as the accuracy of the indent and/or image relies heavily on

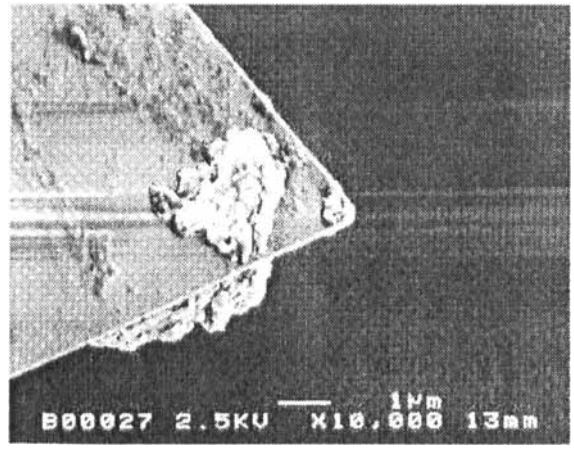

FIGURE 2 A used 90° cube corner tip with radius estimated at 125 nm. Note material deposits on tip that increase area of indentation.

the sharpness/acuteness of the scanning tip with respect to residual indentation features.

The output from these measurements results in two principal values: hardness and indentation modulus. Nanoindentation hardness is an average of material properties and is not a fundamental physical quantity. For many materials, $H \sim 3\sigma y$, and the "Tabor relation" holds where material hardness may be directly related to yield strength [26].

2. EXPERIMENTAL

2.1. Materials

Laminates of several thin foil and bonded configurations were supplied by the Boeing Company according to geometry, surface treatment, aging, and configuration. Table I describes the samples evaluated. Samples were exposed to 204°C thermal aging at ambient atmosphere for time exposure durations of both 1000 and 2000 hours. Additionally, foils were supplied to characterize the interface materials in the "as manufactured" state (Tab. I).

2.2. Sample Preparation

Sample preparation was modeled after the protocol used within the Boeing Company [27] and the final steps were altered to reflect the atomic scale resolution necessary to perform this research. Samples were rough cut (lap shear samples with a diamond wheel cut-off saw) and cured into solid blocks using epoxy resin (Resin 5, Struers, Westlake, OH, USA) and the following sequence was followed to complete the procedure:

(1) Hand sanding using 120 grit wet sandpaper.
(2) Hand sanding using 320 grit wet sandpaper.
(3) Hand sanding using 600 grit wet sandpaper.
(4) Silk wheel (Struers, MD-DAC 200 mm) using 15 μm AlO_3.
(5) Hand polishing using 3 μm diamond paste compound (PSI-503-18, PSI Testing, Houston, TX, USA) on silk cloth (90-150-350, Allied Products, Rancho Dominguez, CA, USA).
(6) Hand polishing using 0.05 μm diamond paste compound (90-21055-S, Allied Products) on silk cloth.

TABLE I Samples evaluated during this study

Sample identifier	*Sample details*	*Environmental history*
SG-1A	15–333 foil, Sol-gel + prime with BRx5	Post-cure at 391°C
SG-2A	15–333 foil, Sol-gel + prime with neat PETI-5	Post-cure at 391°C
SG-4	15–333, sol-gel, no primer	No fabrication or test operations
T1, T2	6–4, sol-gel + PETI-5 lap shear	RT exposure, tested at RT
SG1K400rt	Sol-gel, primed BR-X5, bonded with FM-X5	1000 Hours, 204°C
SG2K400rt	Sol-gel, primed BR-X5, bonded with FM-X5	2000 Hours, 204°C
CrRT-4	Primed BR-X5, FM-X5 lap shear samples	RT exposure
Cr1K400rt	Primed BR-X5, FM-X5 lap shear samples	1000 Hours, 204°C
Cr2K400rt	Primed BR-X5, FM-X5 lap shear samples	2000 Hours, 204°C

Sample indentation and imaging were performed using the following protocol:

(A) Each sample is imaged using SPM to determine flatness and to visualize the area to be indented.
(B) Nanoindentation is performed to obtain "boundaries" of the interface area.
(C) Indentations are performed across the interface.
(D) Sample is imaged using a diamond tip with the indenter in SPM mode.
(E) A high-resolution image of the indented area is acquired using a DI Nanoscope III.

2.3. Interface Characterization

Cross-section nanoindentation analysis of multi-layer interfaces comprised of materials with widely different hardness is a relatively new application of the nanoindentation technique. This is due in part to difficulties in identifying thin layers through laminate cross-section preparation and accurately isolating each layer to achieve an indentation profile. In this study, the adhesion-promoting sol-gel and chromium layers were nominally 1000 Å. Sol-gel varies slightly in thickness as a result of the concentration gradients and the uneven evaporation rate of the carrier.

Images of a sol-gel deposited titanium substrate fractured to fail the sol-gel coating partially were acquired with a Scanning Electron Microscope (JOEL 840, Fig. 3). The coating is inherently brittle; as a consequence, when the substrate is bent to approximately 30°, failure in the coating is initiated.

Transmission Electron Microscopy (JOEL Model 400) has been used to determine the interface thickness of a Titanium/Sol-gel/Primer with the Sol-gel coating of approximately 700 Å in thickness (Fig. 4). While this thickness is adequate to indent, provided the radius of the diamond tip is sufficiently small, the inherent roughness of the titanium substrate (as may be seen in the TEM image) adds to the difficulty of following a relatively straight line of indentation across the interface.

Nanoindentation is highly dependent on the angle at which the diamond tip penetrates the material surface. Indents perpendicular to

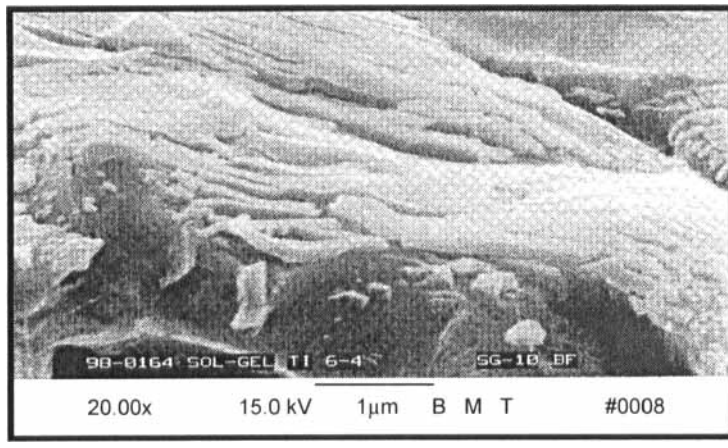

FIGURE 3 Scanning electron microscope image of titanium/sol-gel laminate failed to determine sol-gel thickness.

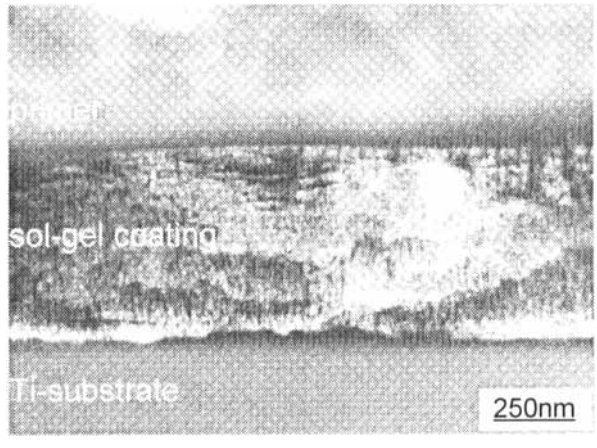

FIGURE 4 Transmission electron microscopy cross-section profile of titanium/sol-gel/primer interface.

the polished material produce optimum results. For this reason, it is critical that extreme care be taken during sample preparation to insure that laminate edges be as flat and parallel as possible. In multi-material cross-sectioned laminates, the relative wear rates of the materials can result in the development of interface troughs and pits. Analysis of the sol-gel and chromium-coated titanium samples indicate that distinct

differences exist between the wear rate of each. In general, chromium exhibits a higher tendency to wear at the polymer interface than sol-gel samples, possibly due to the PETI-5/Chromium exhibiting a lower interfacial adhesion with a contribution from material hardness and modulus differences.

3. RESULTS AND DISCUSSION

3.1. NanoIndentation Standards

Plastic, elastic, and elastic-plastic indentations provide indent curves that are unique and easily identified. Images taken subsequent to indentation of an unknown material combined with characteristic material load-indentation curves enable one to determine explicitly the material composition. Indentation profiles of titanium, sol-gel, chromium, PETI-5 adhesive, and PETI-5 primer were generated from mounted foil samples to obtain profiles of un-aged ("as manufactured") materials. Measurements were performed at indentation depths greater than 20 μm due to the limitations associated with making measurements below this depth. These limitations are not due to instrument resolution but to the natural physical limitations that are the result of both surface asperities and the contact area between two bodies being larger than Hertzian analysis predicts due to surface adhesion forces [28].

Examples of indentation profiles with AFM images and characteristic load-displacement curves are provided in Figure 5. A rigid indentation of titanium (taken with a Berkovich tip) is depicted in the top figure with the characteristic shape and load-displacement profile. Depth sensing indentation is capable of determining mechanical properties of materials with plastic and elastic-plastic behavior [29]. We observe that in titanium there exists a large degree of plastic deformation readily observed in the shape of the unload portion of the load-unload curve. One must take care in depth sensing nanoindentation data interpretation of materials with a high degree of plastic behavior as it has been shown that testing may produce values higher than conventional methods [30]. Additionally, in this case, sample preparation has increased the degree of work

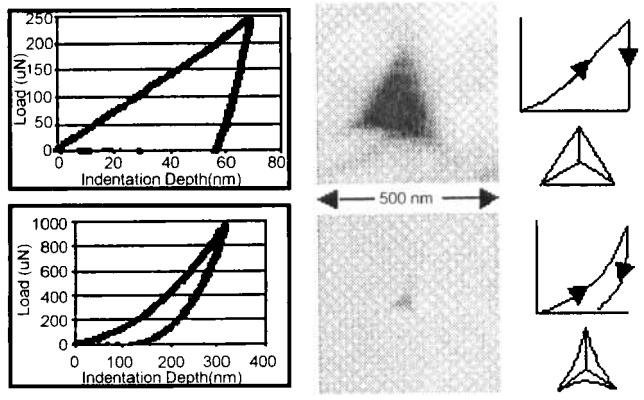

FIGURE 5 Characteristic curves and indentations of perfectly plastic contact (top: titanium) and elastic-plastic contact (bottom: PETI-5 adhesive).

hardening or induced localized stresses that account for the higher properties.

The lower curve in Figure 5 is a load-indentation profile of cured PETI-5 adhesive. PETI-5 exhibits elastic-plastic behavior with a characteristic modulus of between 7–9 GPa. In general, polymer materials are quite challenging to measure using nanoindentation due to difficulties in detecting the surface, viscoelastic behavior, and material damping. In these experiments, we used approach velocities to the polymer surface of 50 nm/second to maximize the strain-rate sensitivity. Due to viscoelasticity it is difficult to obtain stiffness from the slope of the unloading curve making it mandatory to measure a given polymer many times to gain confidence in the values obtained.

Inelastic deformation analysis of titanium is compounded by the formation of the oxide layer that forms on the surface of the substrate [31]. The oxide layer deposited on titanium substrates has been identified using nanoindentation and has been physically measured using Scanning Electron Microscopy (Fig. 6A). Indentations in these surfaces must first overcome the oxide layer that forms on the surface that may exhibit a thickness up to 100 nm. This is highly dependent on several factors including exposure time of the prepared surface, preparation technique, and the specific area analyzed as the oxide layer is not uniform over the entire titanium surface. At times, the oxide

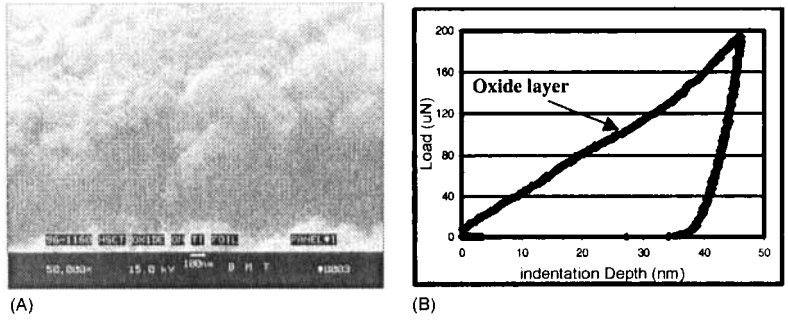

FIGURE 6 Scanning electron micrograph of titanium oxide layer (A) and indentation output (B): Load = 200 μN, Depth = 45 μm.

layer may be registered in the loading curve if the rate of loading is low enough to provide adequate sensitivity. This titanium 6–4 substrate was loaded to 200 μN and a corresponding depth of 45 nm. As is seen by the deviation in the curve (Fig. 6B), this exceeds the limit of the oxide layer resulting in a modulus of 186 GPa, considerably higher than the bulk value reported in the literature of 111 GPa [32]. While it is possible that this is due to a penetration depth that does not exceed the oxide layer, repeated testing to depths up to 200 nm indicate similar results due to the material behavior discussed previously.

Generally, the region of elastic, perfect plastic deformation is contained within a hemispherical zone underneath the indenter, the size of the plastically deformed zone with respect to the contact area being material dependent. Discontinuities are caused by a yield point effect (onset of plastic flow), twinning, cracking or phase transformation [33]. In order to determine the indenter contact area, the assumption is made that the maximum penetration depth is accurate and used to compute the indentation area. This assumption works well for hard materials that work-harden under loading conditions. However, pile-up around the indenter causes the experimental modulus to be higher than the actual macro-measured material modulus due to the underestimation of the contact area as high as 40% [34]. This has been addressed quite readily in analyzing thin films layered on one another using film deposition techniques and is referred to as the "Indentation Size Effect" [35]. Pile-up height is clearly evident in the height profile produced from scanned images, although

the elastic-plastic boundary is usually 3–5x below the maximum indent depth.

Modulus measured at the micro-scale depends heavily on the load applied and corresponding depth of penetration. This is compounded in nano-scale measurements due to several inaccuracies inherent in the values generated as compared with macro-scale measurements [36]. The measurement of 6–4 titanium at several loads and depths clearly indicates that this trend exists (Fig. 7A). As the load value is increased from 100 to 500 μN, the depth increases from 15 nm to nearly 100 nm resulting in a modulus decrease of approximately 15% from 210 to 180 GPa which corresponds to results reported by other research

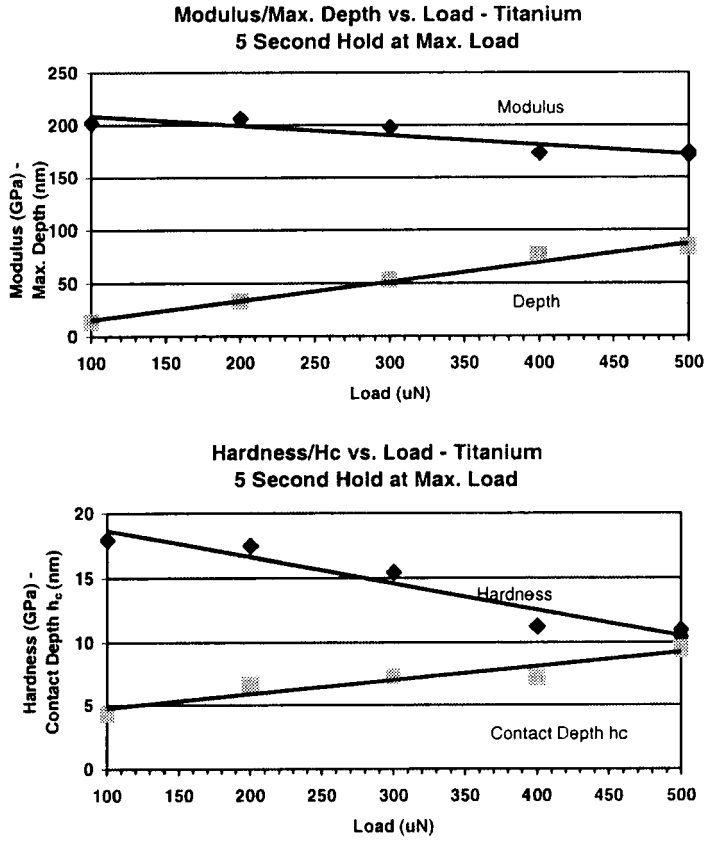

FIGURE 7 Modulus/maximum depth *vs.* load and hardness/h_c *vs.* load: Titanium 6–4.

groups on ferrous material systems [37]. The load was held for 5 seconds to insure accuracy of the data collection and material compliance [36].

Hardness and contact depth compared as a function of load exhibit similar trends (Fig. 7B). Hardness and modulus generally correspond to one another with the contact depth, h_c, being the vertical distance along which the indenter is in contact with the sample material at maximum load. The contact depth is a direct function of the maximum depth, the residual hardness impression, and a constant based on the indenter tip shape. These are computed from the same fundamental values as are used to determine the maximum depth and thus correspond directly. Therefore, material discontinuities that influence nanoscale material values such as the yield point effect, cracking, or twinning, result in the direct hardness and modulus correlation with increasing load.

3.2. Nanoindentation Results – As Manufactured

Characteristic load-depth curves have been developed for aged and "as manufactured" conditions across each interface region. Initially, a Berkovich tip was used at load levels to 1000 mN across interfaces of both un-aged laminates. Subsequently, the interface regions were examined using the indentation tip in SPM mode. An SPM image and corresponding Load-Depth curve for each material group in a titanium/sol-gel interface in the un-aged state is shown in Figure 8. The titanium curve indicates a characteristic step probably due to the presence of an oxide layer while the sol-gel curve indicates a severe incline at 75 nm, perhaps due to interface contributions from neighboring materials causing either slip or low deflection during the loading phase of the indent. This may explain the modulus value of this particular sol-gel test as compared with the majority that measured in the range between 40 – 50 GPa. For comparison, silica samples exhibit modulus values of 68 GPa, understandably higher than silica sol-gel measurements due to the differences in density and morphology.

In Figure 8, the indentations are linear and highly visible near the top of the sample (indentations made in the titanium region), although near the interface and polymer regions indentations are barely visible.

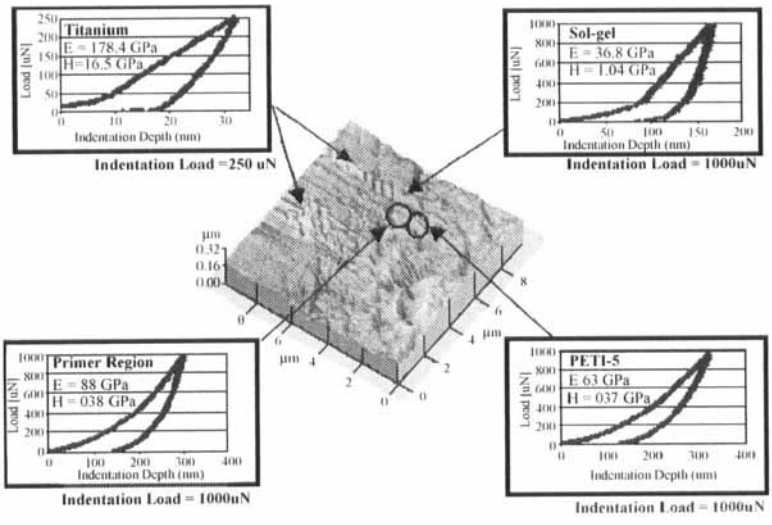

FIGURE 8 Progression of indents across a titanium/sol-gel interface in the "as manufactured", un-aged state (sample SG-2A). Load levels were up to 1000 µN and penetration depths to 300 nm in the polymer-based systems. (See Color Plate I).

This is due to the viscoelastic nature of the polymer region accounting for recovery of the indent signature as well as the inherent roughness of the interface and polymer regions. Nevertheless, one is readily able to follow the path of indentations. Measurements in this sample were made a distance of 2x the indentations diameter apart from one another. This may be too close for accurate measurements, due to plastic deformation. Generally, a rule of thumb is a distance of 5x the diameter of the indent is the closest that progressive indentations should be taken.

3.3. NanoIndentation Results – Aged Samples

Indentation measurements of both sample sets were subsequently performed. Low loads combined with the cube-corner tip allow for sample imprints inherently smaller in area as compared with the Berkovich tip, thus, providing the ability to measure within several hundred Angstroms and remain a distance 4–5 times the sample imprint diameter apart. Figure 9 illustrates a series of chromium interface Load-Displacement plots for interfaces aged 1000 hours

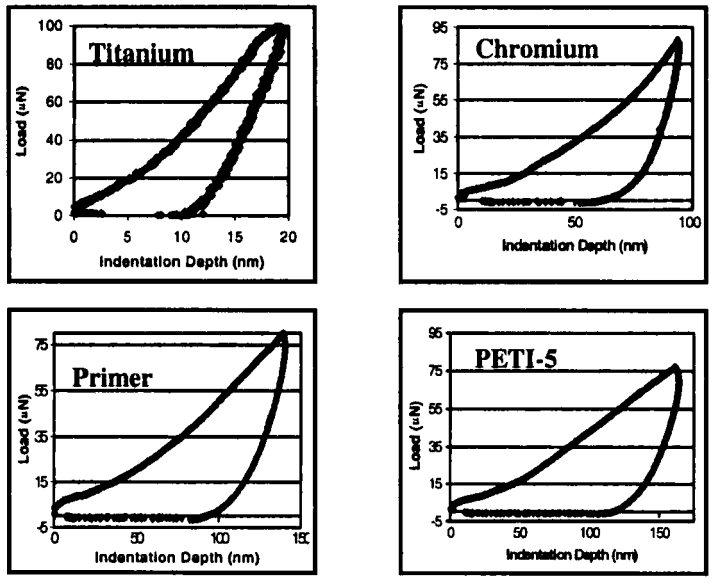

FIGURE 9 Characteristic load-displacement curves of each material at the Titanium/Sol-gel/Primer/PETI-5 adhesive interface aged for 1000 hours. Measured modulus values corresponding are as follows: Titanium 181 GPa, Chromium 32.3 GPa, Primer 11.9 GPa, PETI-5 7.5 GPa.

(Sample Cr1K400rt). The titanium measurement is characteristic of titanium measurements made on other samples, exhibiting the plastic deformation curve characteristic of work-hardened materials. The chromium interface exhibits elastic-plastic behavior that is more pronounced than the primarily elastic sol-gel region. More important is the curve shape of the primer and PETI-5 regions. Clearly the aged sample area under the curve is greater and more closely resembles a plastic nature as compared with the elastic-plastic depicted in the "as manufactured" sample plots. This is likely due to polymer embrittlement, increased cross-linking or chain length reduction as a result of aging. It has been shown that in Nylon the effect of moisture uptake leads to a reduced hardness [34], although it is believed that this polyimide-based psuedo-thermoplastic will not exclusively exhibit thermoplastic behavior.

The unique difference between the load-displacement curves of aged and un-aged polymer samples is related to the effect that aging has on the organic polymeric chains that results in increased plastic behavior.

This phenomenon has been analyzed in other material systems using the classical hardness analysis approach which states that a measured material hardness offers an average pressure of resistance [26] to the indenter, known as the dynamic hardness, numerically equal to the ratio:

$$\frac{\text{Energy of the Indenter}}{\text{Volume of the Indentation}} \tag{3}$$

In nanoindentation, the dynamic hardness may be calculated using a work of indentation approach in which the area enclosed by the loading-unloading curve (the plastic work of indentations) is divided by the residual volume of the indentation impression [38, 39].

3.4. Laminate Analysis

Generally, indentation results obtained across the laminate interface were shifted to compensate for the uneven profile at the interface. Due to the uneven topography of the titanium substrates, there is difficulty in making multiple parallel transverse measurements across the interface. This is compounded by the process variations in both the primer application thickness and the chromium and sol-gel thickness variations in each laminate. SPM images indicate the variation in the sol-gel and topographical discontinuity in the titanium substrate to be significant (Fig. 10). The point selected for measurement across the sol-gel interface is 111.86 nm, although, clearly, the thickness varies across the laminate within this $2\,\mu m \times 2\,\mu m$ image.

Therefore, when plotting multiple measurement sequences on one graph, the X-axis reads in nanometers begins as zero, although these are arbitrary as such measurements are in a relative scale across the laminate. After several indentations are performed, the series of modulus *versus* position values are plotted together and aligned to the inflection point between the PETI-5 primer and coating interface. This position was selected because it is consistently the most accurate point at which to distinguish a modulus and hardness variation.

Modulus values from a single transverse indentation conducted across a chromium laminate in the "a manufactured" condition are provided in Figure 11. Load levels were kept at a constant load of 100 μN and, thus, indentation depths were between 30 nm for titanium

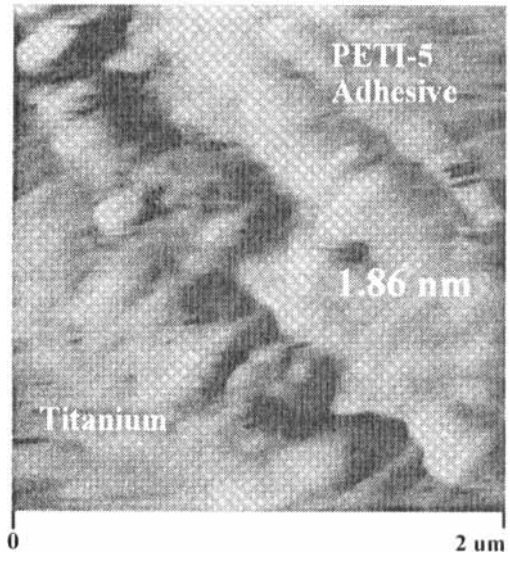

FIGURE 10 Friction force microscopy image of the titanium-sol-gel-primer interface. The distance at the point depicted is 111.86 nm, well within the limits of the manufacturing process.

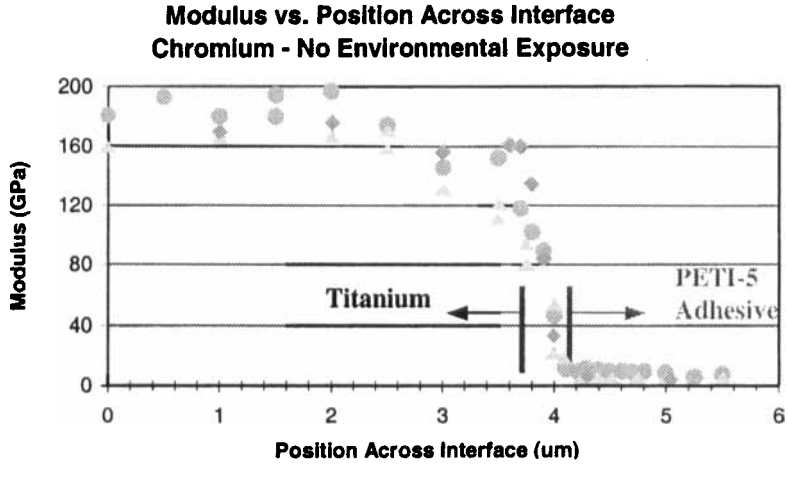

FIGURE 11 Modulus *versus* position along interface (μm) for three measurements conducted transverse to 15-3-3-3 Titanium/Chromium/5 BR-X5 primer/FM-X5 PETI-5 (laminate CrCT-4) laminate and aligned to indicate modulus differences of each material.

up to 130 nm for PETI-5. The distance between indentations was kept to 100 nm or less. In Figure 11 one is able to view the step-wise nature of each material modulus. Clearly, an edge effect exists in the titanium substrate. This could be due to the method by which the laminate was manufactured or perhaps to the processing of the titanium itself. Stress relaxation at the edge could also account for the decrease in modules as the edge of the laminate is approached. This trend exists in all titanium laminates tested, regardless of the thermal aging condition.

Closer analysis of the interface region indicates distinct differences its each constituent material within the laminate (Fig. 12). For example, at this resolution the distinction between the modulus of PETI-5 and PETI-5 primer may be discerned at 7–8 GPa and 10–11 GPa, respectively. Clear modulus deviations exist across the interface. For instance, sol-gel measurements varied up to 8 GPa due to interface effects. Note also that measurements between 0.6 μm and 0.7 μm are likely on the sol-gel-titanium edge, explaining the interface step. To clarify each of these trends, we determined that at least three measurements of each laminate must be performed and compared with standards to obtain a high confidence level in the resultant modulus values.

A compilation of modulus results of several tests conducted across a chromium interface in the three conditions considered reveals that the

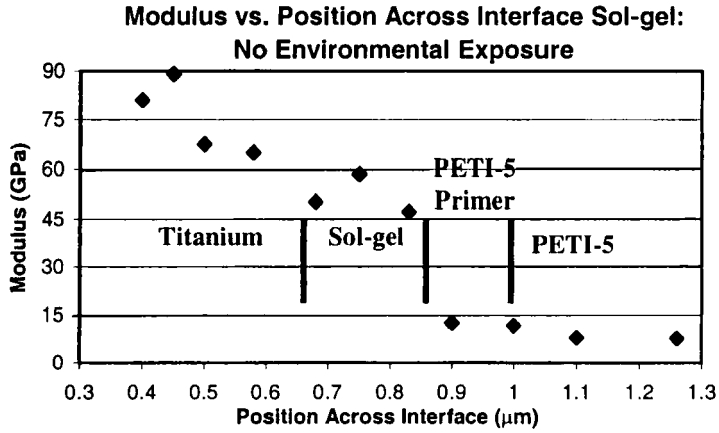

FIGURE 12 Localized analysis of the modulus *vs.* position across a sol-gel, "as manufactured" laminate interface.

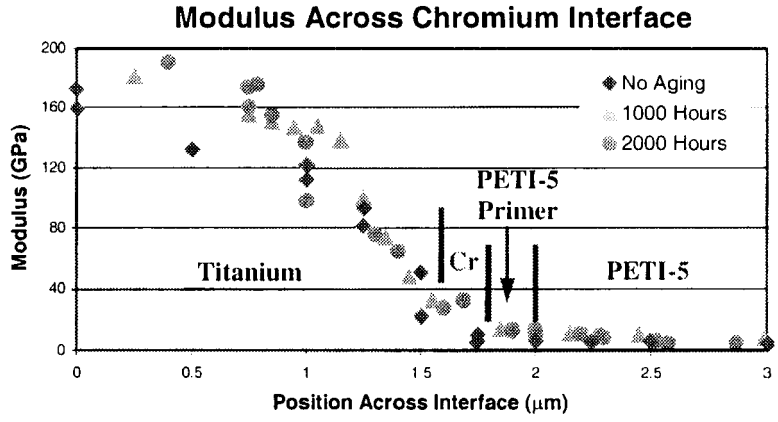

FIGURE 13 Modulus across laminate interface as a function of thermal exposure: Chromium.

effect of aging increases the PETI-5 based primer and adhesive modulus between 20–25%. While the effect on chromium indicates a modulus increase of approximately 15% at 1000 hours, there is a minimal effect between 1000 and 2000 hours. Figure 13 is representative of one test at each exposure level and Table II summarizes the corresponding modulus values.

Modulus results of the sol-gel laminates reveals that there is a similar change in the PETI-5 based polymer materials while the sol-gel polymer interface shows a degradations of approximately 20%. Figure 14 illustrates three representative plots of the individual measurements and Table III summarizes the results of the measurements. Again, as least three measurements were conducted on each interface but, in nearly all cases, several more than three were performed and the results were averaged to arrive at the values published in the tables.

3.5. Measurement of Contact Depth

Measurement of the contact depth may be referred to as a direct relationship with the plastic deformation of a material [40]. Contact depth, represented as h_c, has been determined for both chromium and sol-gel interfaces as a function of environmental exposure. A sample of these measurements in both the chromium and sol-gel

TABLE II Modulus results as a function of aging: Chromium laminate interface

Condition	*Chromium*	*Primer*	*PETI-5*
No Exposure	26–29 GPa	11–13 GPa	7–8.5 GPa
1000 Hours	32–36 GPa	13–14 GPa	8–10 GPa
2000 Hours	34–38 GPa	14–16 GPa	10–11 GPa

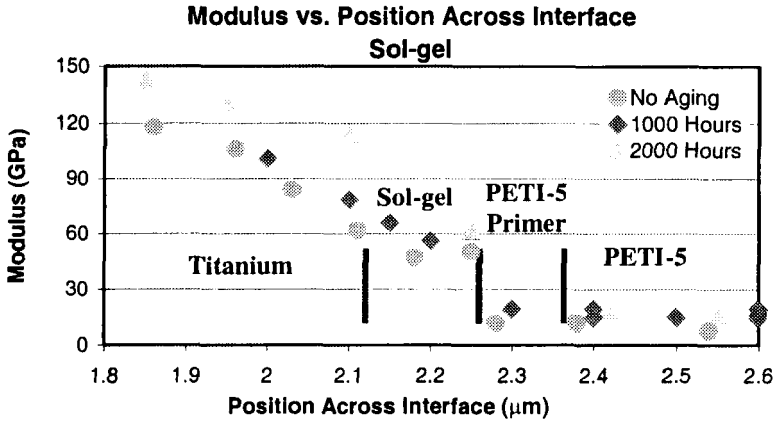

FIGURE 14 Modulus across laminate interface as a function of aging exposure: Sol-gel.

TABLE III Modulus results as a function of aging: Sol-gel interface

Condition	*Sol-Gel*	*Primer*	*PETI-5*
As Manufactured	46–58 GPa	11–13 GPa	7–8.5 GPa
1000 Hours	58–63 GPa	13–15 GPa	8–10 GPa
2000 Hours	58–63 GPa	13–15 GPa	10–12 GPa

systems as a function of aging are depicted in Figures 15 and 16, respectively.

In each, the maximum depth of the aged polyimide-based primer and adhesive decreases by up to 50%, indicating conclusively that chain embrittlement or shrinkage is associated with aging of the laminate. Note, however, that within the polymer, the depth of penetration increases as a function of distance from the titanium-coating hard surface and further into the bulk polymer, regardless of the aging condition. The relationship between the three aging conditions remains the same in both sample cases indicating that the

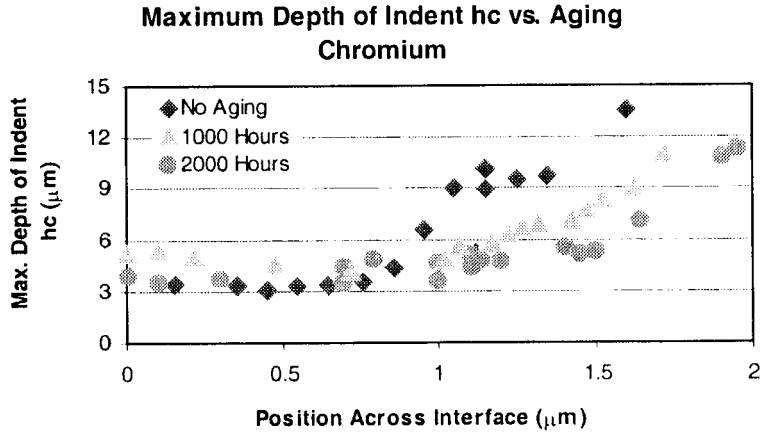

FIGURE 15 Maximum depth of indent, h_c, across chromium interface as a function of thermal exposure.

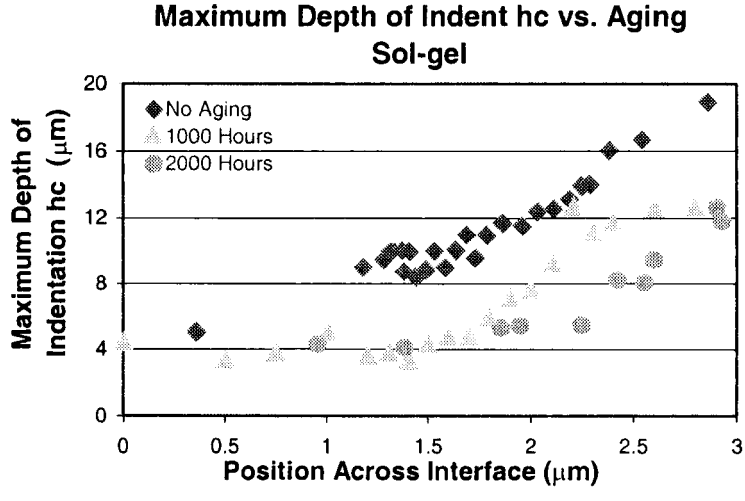

FIGURE 16 Maximum depth of indent, h_c, across sol-gel interface as a function of aging.

trend is repeatable regardless of the coating system on the titanium substrate.

The reduction in contact depth of the PETI-5 adhesive, between 25% and 50%, corresponds to previous results indicating a reduction of Ti-6Al-4V/FM-5 strain energy release rate as a function of aging

(27%) due to the chemical aging/oxidation of the material system in air [14].

As a function of aging, polymeric embrittlement increases with chain rigidity resulting in a lower system free energy. As a result, the modulus increases with a corresponding decrease in system strain, resulting in a contact depth decrease for an identical load and tip geometry. We interpret the modulus increase reported herein to correlate with the decrease in strain energy release rate [14].

Change in modulus and depth of penetration of PETI-5 near the substrate surface is likely due to the constrained mobility of the polymer [41]. Coated titanium influences the segmental mobility and relaxation in the polymer surface due to the adsorption interaction and conformation restriction imposed by the surface [42]. Additionally, polymer structure formation near a surface will be different from the bulk polymer due to changes in molecular mobility. For instance, the density of a polymer near a surface is generally less than in bulk due to time retardation of the relaxation process [43]. It has been shown that the elastic modulus of a polymer increases with decreasing surface-to-volume ratio (*i.e.*, distance to the surface) as a result of decreased chain mobility [44, 45].

Controlling the adhesive morphology near the interface of composites is critical in achieving maximum properties. This is especially true in composite materials with a thermoplastic matrix component where the matrix and composite properties are largely determined by the crystallization of the matrix. The interaction of polymer chains with a solid surface alters the kinetics of crystallization and may also affect nucleation. Studies of crystallization of poly(ether-ether-ketone) (PEEK) under the constraint of reinforcing fibers have shown that nucleation from fibers dominates morphology [46]. Polymer-substrate adsorption interaction may control the crystallization process, as a weak interaction has little effect on crystallization while a strong interaction between solid and polymer slows crystallization considerably [47].

Morphological considerations in thermosetting adhesives may be altered due the change in crosslink density, gel time, molecular weight, molecular weight distribution and rate of polymerization. Any changes in the cure conditions caused by the presence of a reinforcement surface will change the properties of the matrix in the

vicinity of the reinforcement, regardless of whether it is a fiber, metal substrate, or otherwise. A possible explanation is that the small molecule curing agents are depleted in the interphase by adsorption on the reinforcement surface. In contrast, a more restrained interphase can be achieved by using coupling agents that will act as surface-active molecules and retard adsorption of curing agents. While the use of coupling agents with active functionalities may help in polymer-reinforcement bonding, optimization of the interphase crosslink density will ultimately create material compatabilities insuring structural integrity in the presence of large material coefficient of thermal expansion differences under significant, repeated temperature exposures.

4. CONCLUSIONS

Indentation studies of sol-gel coated titanium substrates indicate a pronounced step-wise gradient across the interface continuing well into the titanium laminate (3–4 μm). As compared with un-aged PETI-5 adhesive, aged material increased in modulus on average over 25% after 2000 hours at 204°C, from 8 GPa to 11 GPa, while the primer modulus increase was slightly under 15%. These results appear to contradict previous studies addressing the thermal stability of fully-imidized PETI-5 [48, 49].

Sol-gel increased in modulus after 1000 hours of exposure by approximately 15%, achieving a plateau at this level and showing no signs of modulus deviation with additional aging. Chromium behaved in a different manner. Initially, the un-aged material maintained an average modulus of 27.5 GPa, approximately half that of the sol-gel. More importantly, the modulus gradually rose with aging, rising approximately 25% as a function of aging up to 2000 hours with no plateau visible within the upper limits of the time duration of this study.

The analysis of the maximum indentation depth, h_c, indicates that both laminate configurations exhibit up to a 50% decrease in plastic deformation at the PETI-5 primer/PETI-5 adhesive areas as a function of aging, indicating a decrease in chain mobility, additional polymer embrittlement, and loss of ductility. It is clear that further testing is

necessary to confirm the observations reported herein and that a more comprehensive database must be developed that addresses additional environmental conditions such as moisture, hot-wet conditions, and longer periods of severe environmental exposure.

These results indicate the mechanisms that determine the mechanical performance of complex multi-material structural composites may be analyzed at the nanoscale level and reveal information critical to the long-term system performance. In addition, strain rate sensitivity at the nanoscale, not addressed in this study, could provide additional insight into the overall system performance.

The advantages of studying complex composite laminates at the nanoscate level can not be over-emphasized. The level of mechanical property resolution provides an understanding of the system mechanism behavior that previously has not been available. This is especially important in the areas of mission-critical structures and products that require a long service life under demanding conditions.

Acknowledgements

We wish to express our gratitude to the Boeing Company and to the National Aeronautics and Space Administration for their generous support (High Speed Research Program, NAS1-20220). We thank the NASA CAS ITD Team, NASA Langley Research Center, for the review of this document and Mr. Kevin Pate, HSCT Materials and Processes, Boeing Company, for his patience and guidance during this effort. In addition, we wish to thank Mr. Luther Gammon of the Boeing Company for providing assistance in sample preparation and obtaining a portion of the SEM images. We further acknowledge Dr. Van Eden, Hannesville, WA, and Mr. Hanson Fong, University of Washington Bioceramics Laboratory, for their assistance.

References

[1] Falcone, A., Pate, K. D., Cao, T. Q., Hsu, G. F. and Rogalski, M. E., *Proc. 41st Int. SAMPE Sym.* pp. 1035–1046 (1996).
[2] Smith, J. G. and Hergenrother, P. M., *Poly. Prepr.* **35**, 353–355 (1994).
[3] Hergenrother, P. M. and Smith, J. G. Jr., *Polymer* **35**, 4857 (1994).
[4] Hergenrother, P. M., Bryant, R. G., Jensen, B. J. and Havens, S. J., *J. Polym. Sci., Part A: Polym. Chem.* **32**, 3061 (1994).

[5] Cano, R. J. and Jensen, B. J., *J. Adhesion* **60**, 113 (1997).
[6] Allen, M. R., *NASA-CR-198193* (1995).
[7] Boyer, R. R., *J. of Mat.* **5**, 23–25 (1992).
[8] *Adv. Mat. and Proc.* **3**, 39 (1999).
[9] Kinloch, A. J., *J. Adhesion* **10**, 193–210 (1979).
[10] Daghyani, H. R., Ye, L. and Mai, Y. W., *J. Mat. Sci.* **31**, 2523–2529 (1996).
[11] Watts, J. F., Castle, J. E. and Hall, T. J., *J. Mat. Sci. Letters* **31**, 2523–2529 (1988).
[12] Wang, J. Z., Parvatareddy, H., Chang, T., Iyengar, N., Dilard, D. A. and Reifsnider, K. L., *Comp. Sci. Tech.* **54**, 405–415 (1995).
[13] Sullivan, J. L., Blais, E. J. and Houston, D., *Comp. Sci. Tech.* **47**, 289–305 (1993).
[14] Parvatareddy, H., Dillard, J. G., Mcgrath, J. E. and Dillard, D. A., *J. Ad. Sci. Tech.* **12**, 615–627 (1998).
[15] Bhushan, B., Israelachvili, J. N. and Landman, U., *Nature* **374**, 607 (1995).
[16] Consiglio, R., Randall, N. X., Bellaton, B. and Von Stebut, J., *Thin Solid Films* **332**, 151 (1998).
[17] Gerberich, W. W., Nelson, J. C., Lilleoden, E. T., Anderson, P. and Wyrobek, J. T., *Phil. Mag. A* **74**, 1117 (1996).
[18] Holbery, J. D., Eden, V. L., Sarikaya, M. and Fisher, R. M., *Rev. Sci. Inst.* **71**, 3769–3776 (2000).
[19] Bulychev, S. I. and Alekhin, V. P., *Zavod. Lab.* **41**, 1137 (1975).
[20] Doerner, M. F. and Nix, W. D., *J. of Mat. Res.* **1**, 601 (1986).
[21] Oliver, W. C. and Pharr, G. M., *J. of Mat. Res.* **7**, 1564 (1992).
[22] Sneddon, I. N., *Int. J. Engin. Sci.* **3**, 47 (1965).
[23] Johnson, K. L., In: *Contact Mechanics* (Cambridge Univ. Press, Cambridge, 1989).
[24] Gerberich, W. W., Yu, W., Kramer, D., Strijny, A., Bahr, D., Lilleodden, E. and Nelson, J., *J. Mat. Res.* **13**(2), 421–439 (1998).
[25] Baker, S. P., In: *Nanoindentation Aspects, Tutorial Notes*, MRS Spring 1998 Meeting, Symp. T-Tutorial.
[26] Tabor, D., In: *The Hardness of Metals* (Oxford Univ. Press, London, 1951).
[27] Gammon, L. M. and Ray, D. J., In: *Proc. 30th IMS Conv.*, Seattle, WA, July 20–25, 1997.
[28] Bahr, D. F., Kramer, D. E. and Gerberich, W. W., *Acta Mater.* **46**(10), 3605–3617 (1998).
[29] Bahr, D. F., Watkins, C. M., Kramer, D. E. and Gerberich, W. W., In: *Fundamentals of Nanoindentation and Nanotribology.*, In: *MRS Symp. Proc. V.* 522, Moody, N. R., Gerberich, W. W., Burnam, N. and Baker, S. P. Eds., pp. 83–88 (1998).
[30] Randall, N. X. and Julia-Schmultz, C., In: *MRS Symp. Proc. V. 522*, Moody, N. R., Gerberich, W. W., Burnam, N. and Baker, S. P. Eds., pp. 21–26 (1998).
[31] Johnson, Kendall and Roberts, *Proc. R. Soc. Lond. A.* **324**, 301–313 (1971).
[32] Felback, D. K. and Atkins, A. G., In: *Strength and Facture of Engineering Solids* (Prentice-Hall, New York, 1984).
[33] Mchargue, C. J., In: *Micro/Nanotribology and its Applications*, Bhushan, B. Ed. (Kluwer Pubs., Amsterdam, 1997), pp. 467–492.
[34] Bolshakov, A., Oliver, W. C. and Pharr, G. M., In: *Mat. Res. Symp. Proc.* MRS, V. **436**, 141–146 (1997).
[35] Briscoe, B. J., Sebastian, K. S. and Sinha, S. K., *Phil. Mag. A.* **74**(5), 1159–1169 (1996).
[36] Tsui, T. Y., Oliver, W. C. and Pharr, G. M., In: *MRS Symp. Proc*, V. **436**, 147–152 (1997).
[37] Castell, M. R., Shafirstein, G. and Ritchie, D. A., *Phil. Mag. A* **74**(5), 1185–1195 (1996).
[38] Stilwell, N. A. and Tabor, D., *Proc. Phys. Soc.* **78**, 169–179 (1961).
[39] Hains Worth, S. V., Sjostrom, H., Page, T. F. and Sundgren, J. E., In: *MRS Symp. Proc V.* **436** (1997).

[40] Wang, H. F., Nelson, J. C., Gerberich, W. W. and Deve, H. E., *Acta Metall. Mater.* **42**(3), 695–700 (1994).
[41] Miller, J. D. and Ishida, H., In: *Fundamentals of Adhesion* Lee, L. H. Ed. (Plenum Press, NY, 1992), p. 291.
[42] Lipatov, Y. A., *Rubber Chem. Tech.* **49**, 1311 (1976).
[43] Lipatov, Y. A., *Trans. Int. Plast. Ind.* **4**, 83 (1966).
[44] Lipatov, Y. S., *Polymer* **16**, 582 (1975).
[45] Lipatov, Y. S. and Babich, V., *Vysokomol Soedin.* **10**, 848 (1968).
[46] Peacock, J. A., Fife, B., Nield, E. and Crick, R. A., In: *Composite Interfaces*, Ishida, H. and Koenig, J. L. Eds. (Elsevier, Amsterdam, 1986).
[47] Lipatov, Y. S., *Physical Chemistry of Filled Polymers* (Rubber and Plastics Assoc. of Great Britain, England, 1979).
[48] Cho, D. and Drzal, L. T., *J. Appl. Poly. Sci.* **76**, 190–200 (2000).
[49] Cho, D. and Drzal, L. T., *J. Appl. Poly. Sci.* **75**, 1278–1284 (2000).